Received: 20 February 2024 | Revised: 25 June 2024 | Accepted: 22 July 2024

DOI: 10.1111/jace.20080

Journal of the American Ceramic Society

REVIEW ARTICLE

Impact of volatility, non-stoichiometry, and atmospheres in perovskite piezoelectric and dielectric materials

Clive A. Randall[1] | **Hiroshi Nishiyama**[1,2] | **Hiroyuki Shimizu**[2]

[1]Department of Materials Science and Engineering, The Pennsylvania State University, University Park, PA, USA

[2]R&D Center, TAIYO YUDEN CO., LTD., 5607-2 Nakamuroda, Takasaki 370-3347, Gunma, Japan

Correspondence
Hiroshi Nishiyama, Department of Materials Science and Engineering, The Pennsylvania State University, University Park, PA, 16802, USA.
Email: h-nishiyama@jty.yuden.co.jp

Funding information
National Science Foundation, Grant/Award Numbers: 1841453, 1841466

Abstract

Defect chemistry that results in the thermal processing of dielectric and piezoelectric films, crystals and ceramics ultimately controls the properties and long-term performance of materials and devices. This paper reviews several thermochemical defect reactions using important perovskite base composition dielectrics including $Pb(Zr,Ti)O_3$, $(Na,K)NbO_3$, $(Bi_{0.5}Na_{0.5})TiO_3$–$BaTiO_3$, and $Ca(Hf,Ti,Mn)O_3$. Within this group of perovskite-based functional materials, we note ways the point defects can be formed to create non-stoichiometric compositions changing the overall cation-to-anion ratios during the synthesis process. These reactions can be developed with the loss of volatile species such as metal and oxygen ions. The relative concentrations of these can impact the over conductions in terms of the mixed contributions of ionic conductivity from the oxygen vacancies and the electronic conductivity, along with microstructure and properties in some cases.

KEYWORDS
defects, dielectric materials/properties, lead-free ceramics, piezoelectric materials/properties, volatilization

1 | INTRODUCTION

Dielectric and piezoelectric ceramics are an important group of materials that are prepared with thermal energy and produced in both thin films and ceramics. Under the thermal processes, materials can undergo crystallization, densification, or grain growth.[1–3] Under these processing conditions, the point defect species and their concentrations are formed and attempt to equilibrate with the temperature and the atmospheres.[4–6] The processing time and temperature, along with the grain size and sample size, also determine the diffusional mechanisms of these processes, and so the time at a specific temperature will determine the defect concentrations and spatial distribution of these defects within the material. Given these dynamic changes, it is important to understand the many ways in which a material can be processed and to develop the underlining defect chemistry that impacts the resulting electrical properties. These properties reflect the elasto-dielectric nature of the material, and they vary with time, temperature, stress, electric field, and frequency.

Point defects are a natural thermodynamic occurring process, and in all materials, there are intrinsic defect reactions that maintain the stoichiometry through Schottky or Frenkel reactions. The Schottky reaction gives a balance of the metal and oxygen vacancies in accordance with the cation-to-anion ratios of the composition. This stoichiometric ratio is also maintained with the Frenkel

reactions, as the crystal structure has sufficient space to permit cations (or anions) to occupy interstitial positions. With the perovskite and its close packed structure, the Schottky defects are important. These reactions are present and will be in equilibrium with other reactions that are non-stoichiometric and these change the cation-to-anion ratio within the perovskite and are the focus of this review.[7–9,10–12]

Many of the important perovskite materials of interest for dielectric and piezoelectric applications have compositions with species that are volatile. The perovskites have the nominal formulation of ABO_3, with the A-site having a 12-fold coordinated sites and the B-site having octahedral coordination. In the processing of such materials in single crystal growth, calcination of powders, sintering powders into dense ceramics or driving crystallization with thin film deposition, there is also a loss of volatile elemental species. These volatiles can be metal and/or oxygen species. Therefore, the defect chemistry in the dielectric and piezoelectric materials can have a major impact on the properties and long-term performance of these materials in devices. The objective of this review is to provide some recent insights in understanding of the point defects that can change in the sintering process are of primary importance in designing such materials.[13,14]

Within the thermal processing environment, these volatile species undergo sublimation from the solid phase to the gas phase, which can leave an incongruent compositional stoichiometry relative to the intended engineered composition. An equilibrium vapor pressure is set up and corresponds to the pressure reached when a condensed phase is in equilibrium with its own vapor. This corresponds to the rate at which the sublimation from the ceramic matches the rate of deposition of its vapor phase back into the solid. The most volatile metallic species that can make up the compositional design will be an important contributor to the non-stoichiometric chemistry. The most volatile metallic species are in different parts of the periodic table; the volatile metal species in the transition metals from groups 11 and 12 include elements such as Cu, Zn, Ag, and Cd and from groups 13, 14, and 15 include Ga, Sn, Pb, Bi, and Sb, and the alkali metal elements Li, Na, K, Rb, and Cs. Therefore, any of these elements in a composition will lead to non-stoichiometry under the thermal processes.[15,16]

For A-site with highly volatile species relative to more stable cations in the B-site of the perovskite, ABO_3 can have the following reactions:

$$(AO)(BO_2)\ (s) \leftrightarrow x(AO)\ (g)\uparrow + (AO)_{1-x}(BO_2)\ (s) \quad (1)$$

or

$$(AO)(BO_2)\ (s) \leftrightarrow x(AO_{1-n})\ (g)\uparrow + \frac{n}{2}O_2\ (g)\uparrow + A_{1-x}BO_{3-(x+n)}\ (s) \quad (2)$$

Equation (1) considers the volatile AO species with a congruent associative loss and Equation (2) considers the dissociative volatility based on an A-site metal suboxide, respectively. An associative reaction maintains the stoichiometric ratio of the metal to oxygen ratio, whereas the dissociative reaction involves a reduction to a suboxide with the volatile metal species, and the release of the oxygen species. In either case, this A-site volatile leads to an A-site-deficient chemistry relative to the B-site, so we will generate metal vacancies on the A-site and oxygen vacancies on the anion site.

In contrast, if the higher volatility is associated with the B-site relative to the A-site, we can have the following reactions:

$$\begin{gathered}(AO)(BO_2)\ (s) \leftrightarrow x(BO_2)(g)\uparrow + (AO)(BO_2)_{1-x}\ (s)\\ (AO)(BO_2)\ (s) \leftrightarrow x(BO_2)\ (g)\uparrow + AB_{1-x}O_{3-2x}\ (s)\end{gathered} \quad (3)$$

or

$$(AO)(BO_2)\ (s) \leftrightarrow + (AO)(BO_2)_{1-x}\ (s) + x(BO_{2-n})\ (g)\uparrow + \frac{xn}{2}O_2\ (g)\uparrow \quad (4)$$

In addition to the cation volatility, the oxygen anion is also a volatile component that can lead to a reduction or an oxidation reaction with respect to sintering and annealing atmospheres, as given in Equations (5) and (6).

$$O_O^{\times} \leftrightarrow \frac{1}{2}O_2\ (g) + V_O^{\cdot\cdot} + 2e' \quad (5)$$

$$\frac{1}{2}O_2\ (g) + V_O^{\cdot\cdot} \leftrightarrow O_O^{\times} + 2h^{\cdot} \quad (6)$$

So, in all these general cases, there is a non-stoichiometry developed with generation of metal and oxygen vacancies associated with the sublimation of the volatile species. Equations (5) and (6) must also be considered with volatile reactions such as Equations (2) and (4). Below, we will consider these specific non-stoichiometric effects with the thermal processes in a variety of important dielectric and piezoelectric perovskite materials. We will consider these materials under both air and low partial pressure sintering or annealing. These changes and the underlying defect chemistry impact the overall conductivity, which is made up of both ionic and electronic conductivity mechanisms, so-called mixed conduction. In the perovskite discussed here, the ionic conduction results from the migration of oxygen vacancies, and the electronic contribution is mostly through the thermal excitation, with the large activation energy of the resistivity across the bandgap from the valence band and donor or acceptor levels to appropriate conduction band. Although there

are different mobilities, concentrations, and activation energies, these collectively contribute to the electrical impedance and they can be experimentally determined from the impedance spectroscopy measurements.[17–20] Other, electrical properties are also impacted from these changes in point defect concentrations, and these can limit the overall performance of these dielectric and piezoelectric materials and components.[21–24]

Above, we have discussed the possibility to form point defects under the thermal processing, and after the generation of defects, there can be re-oxidation with the uptake of oxygen to remove the oxygen vacancies. This re-oxidation occurs at intermediate temperatures particularly on cooling in a furnace.[25,26] For the remaining oxygen vacancies, there can be additional dynamics with respect to the electrostatic interaction. So, at low temperatures (around room temperature), there is a Coulombic interaction between the opposite charges on the oxygen vacancies and acceptor centers including metal vacancies. This interaction creates defect complexes, and these act as defect dipoles that can interact and perturb the ferroelectric polarization and domain wall dynamics. With decreasing thermal energy, the electrostatic attraction can form various configurations with both nearest and next-nearest neighbor interactions and form defect associations or distribution defect dipole complexes. At higher temperatures or under an electric field, these defect complexes can dissociate with the oxygen vacancy moving away from the acceptor point defect centers. These acceptors can be with A-site dopants such as Na and K and B-site dopants can be with Cu, Fe, and Mn in $Pb(Zr,Ti)O_3$ (PZT) or other systems. Details of these dopant interactions and the Coulombic interaction between the volatile species of oxygen and metal vacancies are available in references.[27–30] These and other papers point out the complexities of these associated defect configurations. So, at low temperatures, there are association interactions that can occur and develop local stabilization of spontaneous polarization in the ferroelectric state. This then inhibits the rotational motion of spontaneous polarization in the ferroelectric domain (domain wall pinning effect). In ferroelectrics with aging, ferroelectric domain wall motion is suppressed and results in lower dielectric losses and reduced piezoelectric properties.[31–33] These locally trapped oxygen vacancies can be observed by various techniques, such as electron paramagnetic resonance and thermally stimulated current to understand the dissociation and reorientation processes.[30,34,35] Further insight into these associations can be modeled with first-principles calculations of the coordination of defect complexes with lead vacancies and oxygen vacancies as reported in $PbTiO_3$ system.[36]

Since O^{2-} ions and their associated vacancies move slowly at room temperature, the aging process in ferroelectrics takes several days, weeks, and months to complete. The aging is more advanced when the temperature is raised to 200°C (>Curie temperature 120°C–130°C in $BaTiO_3$, for example)[26] under solid-state sintering; samples are typically air-cooled from the firing temperature to room temperature at about 5°C/min, a rate used to avoid leaving residual stress inside the sample. In contrast, when samples are rapidly cooled from the firing temperature to room temperature, the oxygen vacancies are not compensated and are locally "frozen" to room temperature. This rapid cooling throughout the intermediate temperature regimes, gives a process called "quenching." The quench limits the kinetics of the re-oxidation, but it can also limit the formation of associated defect pairs. As an example, when quenching a hard-type $Pb(Zr,Ti)O_3$ from the firing temperature to room temperature, oxygen vacancies cannot move to the proximity of acceptor defects centers; therefore, the defect dipoles concentrations are at a minimum. This is why the aging process is time sensitive to the dielectric and piezoelectric properties. This aging process typically relates to the defect dipoles stabilizing the spontaneous polarization of the ferroelectric materials.[37,38] Recently, in textured hard piezoelectric materials, it was demonstrated that heating these materials above the Curie temperature and then doing a rapid quench in water results in a quenching process that has large number of dissociated and randomized defects.[39] Then, on poling with an external electric field, the domains more easily realign and high levels of domain alignment can be obtained, giving high piezoelectric coefficients and high mechanical quality factors in piezoelectric materials. Therefore, the strengths of hard and soft piezoelectric ceramics can be combined in a unique process in which defects and their associations are considered.

2 | EXAMPLES OF DIELECTRIC AND PIEZOELECTRIC CERAMICS

Below we will consider specific materials and point out the most volatile species and the basic defect chemistry in each case.

2.1 | $Pb(Zr,Ti)O_3$ case

In sintering, PZT without control of the PbO atmosphere results a loss of PbO, which can impact the grain size, density, intergranular PbO secondary phases, and electrical properties. Sintering of PZT in an O_2 atmosphere enhances the formation of the A-site vacancy (V''_{Pb}) in the perovskite structure, which in turn impacts properties such as increasing the dielectric constant, elastic compliance, and

the piezoelectric coupling factor of the sintered body.[40–42] On the other hand, sintering in N_2 atmospheres leads to the enhanced formation of the oxygen vacancy ($V_O^{\cdot\cdot}$). The ferroelectric and piezoelectric properties are influenced from this stoichiometric change. With increasing $[V_O^{\cdot\cdot}]$, the mechanical quality factor and coercive field both increase.[41] There is also limited grain growth, so size effect can also support the piezoelectric coefficient and relative permittivity.[41] To counter the loss of PbO, either excess PbO can be batched into the materials prior to sintering, but the most effective method is to use source powders of PbO and ZrO_2 to control the PbO activity in the sintering atmosphere. The components of both Pb and O are volatile at calcination and sintering temperatures, and at these temperatures, the Zr and Ti equilibrium vapor pressures are very low. To maintain and control the stoichiometry in such compositions with such different vapor pressures it is important to minimize the departures from stoichiometry. To control the PbO activity, kiln furniture or crucibles that have already been "seasoned" with PbO and source powders are used. This is to make sure that there is limited loss of the PbO from the PZT samples as the PbO activity will equilibrate with all these surfaces in the thermal processing environment. Earlier, Atkin and Fulrath and Holman and Fulrath determined the activity of PbO in the PZT system via an experimental thermodynamic study.[13,43] These researchers were performed over different phase mixtures and different Zr/Ti ratios. It was found that the lead oxide activity varies with the Zr/Ti ratio, and $PbZrO_3$ as a source powder is the easiest to decompose; therefore, it is the best source for increasing the a(PbO). As later pointed out by Kingon and Clarke, absolute control of a(PbO) is difficult and best controlled with respect to the sintering environment that is set up.[44–46] There have been several important processing studies that are used to control the densification and lead stoichiometry in PZT ceramics.[5–28]

The loss of PbO during the sintering process was in accordance with the following reaction:

$$Pb_{Pb}^{\times} + O_O^{\times} \rightarrow V_{Pb}'' + V_O^{\cdot\cdot} + PbO \uparrow \quad (7)$$

At high temperatures, we expect there to be a compensation and the concentration of the oxygen and metal vacancies are balanced under the electroneutrality condition from the Brouwer approximation[47,48] such that:

$$2\left[V_{Pb}''\right] \sim 2\left[V_O^{\cdot\cdot}\right] \quad (8)$$

The mass action Equation (7) becomes:

$$K = \left[V_{Pb}''\right]\left[V_O^{\cdot\cdot}\right] a\,(PbO) \quad (9)$$

On cooling in a furnace with an air atmosphere, for example, there is an uptake of oxygen into the ceramic via Equation (6).

This then changes the ionically compensated defect chemistry to an electronic compensation of the metal vacancy concentration with an electronic hole concentration. Therefore, the compensation can be approximated as, and sometimes this is known as super oxidation process:

$$2\left[V_{Pb}''\right] \sim p \quad (10)$$

Therefore, when processing PZT, we have to be aware with that there are dynamic changes in the PbO loss and the re-oxidation on cooling during the sintering process, which rewrites the controlling defect chemistry.[40,49–53]

Earlier, Donnelly et al. demonstrated in situ changes in impedance spectroscopy measurements of Nb-doped PZT with different oxygen and lead oxide atmosphere (Figure 1). Note that when a buried capacitor structure is used, as shown in Figure 1D, we can elucidate the nature of the conductivity and monitor the rate-limiting process of the PbO volatilization. This multilayer configuration also limited artifacts from short-circuit effects at the sides of the dielectric layer that can occur with a simple parallel plate capacitor structure.[54–57] The equivalent circuit and impedance and admittance spectroscopy data representation could be monitored at elevated temperatures, as shown in Figure 1.

Figure 1A shows the equivalent circuit that effectively has three parallel rails, the first being the capacitance, the second being the electronic conduction, and the third is an ionic rail with a Warburg element and double layer capacitance. A Warburg diffusion element (Z_W) has a constant phase of 45° and with a magnitude inversely proportional to the square root of the frequency. This third rail represents the ionic diffusion of the oxygen vacancies and their accumulation to form ionic space charge with the blocking metal electrodes. Under this condition, there are two relaxation conditions associated with each of the carrier types; therefore, we can separate out the electronic and ionic conductivity, in either the Cole–Cole plot in impedance or admittance representations shown in Figure 1B,C. Figure 2A shows the time evolution of the admittance Cole–Cole plot for $Pb_{1-0.5x}[(Zr_{0.53}Ti_{0.47})_{1-x}Nb_x]O_3$ ($x = 0.0075$) buried capacitor annealed at 700°C for 5, 10, and 32 h, respectively. Prior to the measurement, the buried capacitors are annealed in a PbO source to minimize the metal vacancy concentration, and then within an air atmosphere at 700°C, there is an increase in the ionic conductivity accompanied by a decrease in the electronic conductivity, which means that we are losing the hole concentration. Figure 2B shows the summary of the impact of annealing and the

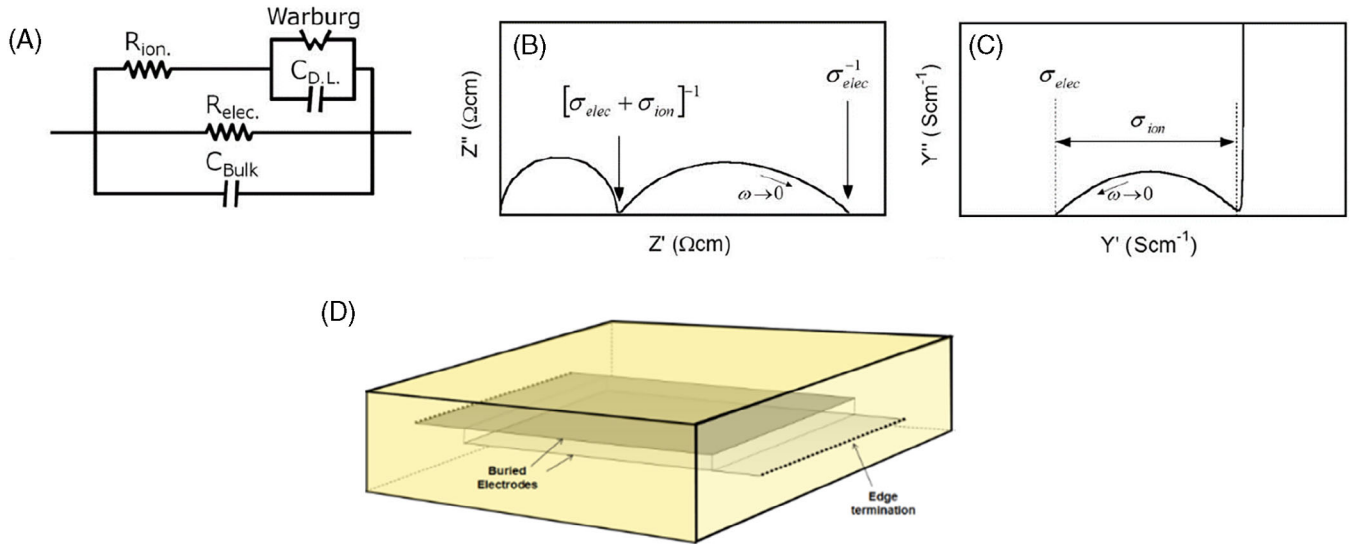

FIGURE 1 (A) An effective equivalent circuit used to model mixed conduction with ion blocking electrodes; (B) simulated impedance spectrum; (C) simulated admittance spectrum. Reprinted with permission. Copyright 2010 AIP Publishing.[55] (D) Schematic of the $Pb(Zr,Ti)O_3$ (PZT) fabricated into a multilayer with embedded electrodes (Reprinted with permission. Copyright 2012 IEEE).[47]

donor doping dependences on the mixed electronic and ionic conductivity. At the initial air annealing, the ionic conductivity rapidly increase and the electronic conductivity decrease, as shown in Figure 2A. Note that, the increasing Nb concentration suppresses the p-type behavior due to the charge neutrality, as shown in Figure 2B. When the annealing atmosphere is changed to the reduced atmosphere, in contrast, the amount of $[V_O^{\cdot\cdot}]$ can be increased via the approximation of $[V_O^{\cdot\cdot}] \gg [V''_{Pb}]$, which can be occurred with Equation (5).[47,48] At the same time, further suppression of the p-type conduction can be explained with the charge neutrality caused by Equation (5). Interestingly, after the second PbO annealing, the defect chemistry is reset and follow the same trend in the air and N_2 annealing, as explained above. In the case of cooling down in air, the increased $[V''_{Pb}]$ is substituted by 2p, which is called re-oxidation.

In low p_{O_2} annealing with nitrogen, this increases the oxygen vacancy concentration, but shows the loss of the PbO at a reduced rate. With the nitrogen anneal there is a loss of oxygen to increase, but this is to be in equilibrium with the mass action reaction Equation (9), and in doing, it will suppress the metal vacancy formation and reduces the rate of the volatility reaction.

So, the PZT ceramics can have their non-stoichiometry impacted within three processing variables of the PbO atmosphere, the oxygen partial pressure, and the temperature with respect to cooling, heating, and holding times. Metastable states can occur concerning the processing; therefore, in designing these processes all these above reactions need to be carefully considered.

2.2 | $NaNbO_3$ and $(Na,K)NbO_3$ cases

These ceramics are of interest for new high-voltage–high-temperature dielectrics and lead-free piezoelectric materials.[58–60] In the sintering of these materials, the volatile species are alkali metals, namely sodium, potassium, and oxygen. Therefore, fast sintering methods that limit the volatility such as two-step sintering, hot press, spark plasma sintering, and cold sintering have been successfully applied.[61–65] The volatility as determined from the equilibrium vapor pressures in the $NaNbO_3$ and $(Na,K)NbO_3$ of the alkali metal oxide species is lower than that in the $Pb(Zr,Ti)O_3$ case. As has been determined by a comprehensive investigation by Malič et al., the equilibrium pressures were experimentally quantified with a Knudsen effusion mass spectroscopy method. The data across multiple perovskite systems are summarized in Figure 3.[66,67] The Knudsen cell methodology is described by Popovič et al.[67]

As can be noted in Figure 3, the alkali oxides and PbO vapor pressures are relatively high, but when contrasted with mixtures of oxides and the perovskite or other oxides, the vapor pressures can be significantly reduced. In comparing the PZT + ZrO_2, which is typically used as a very good PbO source powder for controlling the a(PbO), this is still at a much higher vapor pressure than the alkali oxide-based perovskite with K and Na losses. We also note that comparatively the vapor pressure of $KNbO_3$ is greater than that of $NaNbO_3$ by about an order of magnitude. We would expect that $NaNbO_3$ will have less vacancies than those in $KNbO_3$ in a sintering

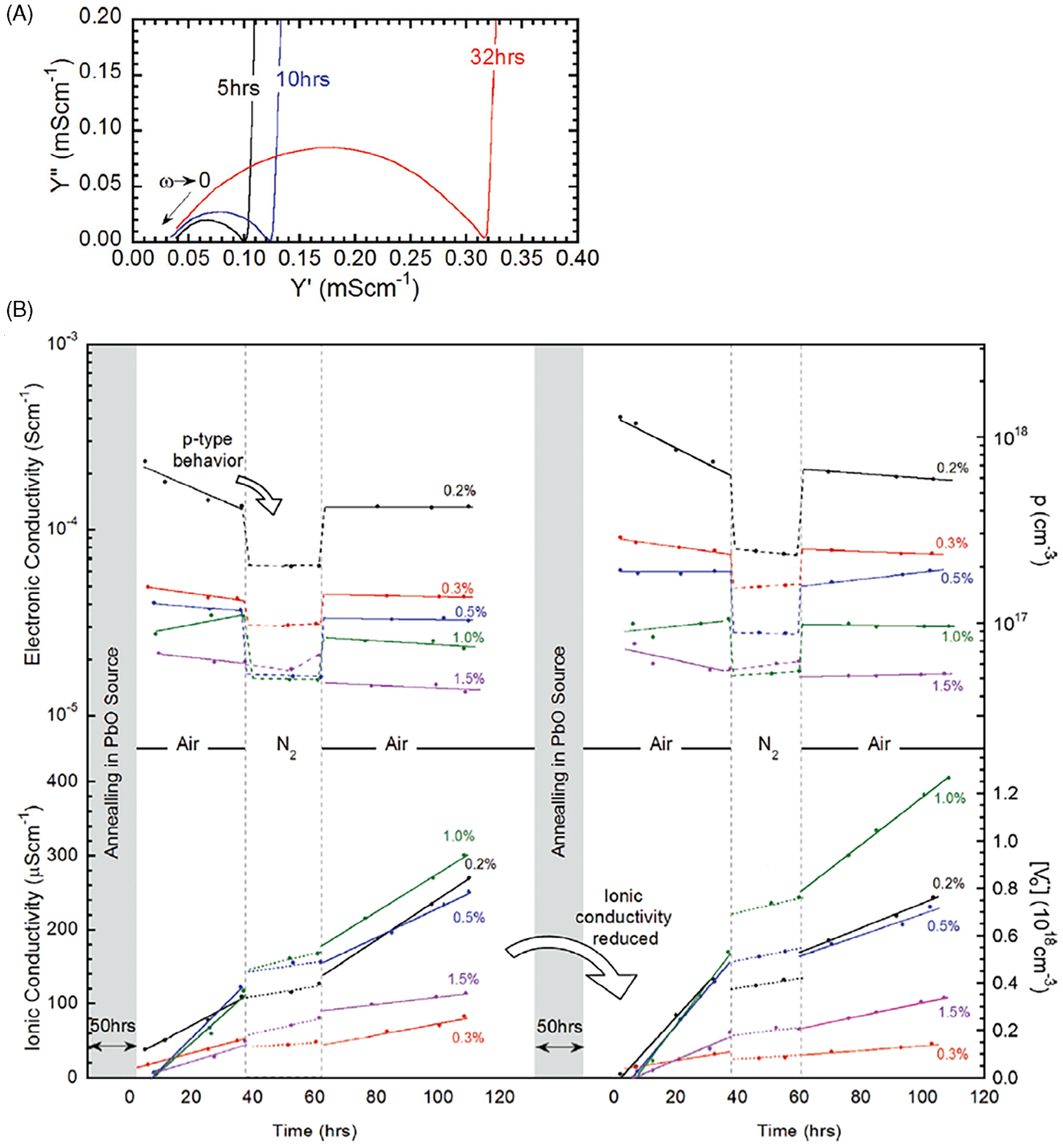

FIGURE 2 (A) Variation in the admittance Cole–Cole curve as a function of annealing in air at 700°C. (B) The extracted electronic and ionic conductivities of $Pb(Zr,Ti)O_3$ (PZT)–*x*Nb buried capacitor structures as a function of annealing time at 700°C (lines are simply guides for the eye). The electronic transition between different p_{O_2} conditions occurs in seconds at this temperature and is simply represented as a step change here. Carrier concentrations are calculated using mobility values from literature. Reprinted with permission. Copyright 2011 AIP Publishing.[54]

process. The $NaNbO_3$ and $(Na,K)NbO_3$ volatility reaction is given by:

$$2\,M_M^{\times} + O_O^{\times} \leftrightarrow M_2O \uparrow + 2V_M' + V_O^{\cdot\cdot} \qquad (11)$$

where the M indicate alkali metals, Na and K. To realize the alkali volatilization effect on $(Na,K)NbO_3$ ceramics, Nishiyama et al. demonstrated the impact of an intentional annealing in air on a sintered body.[68] The intentional annealing at 1000°C of stoichiometric

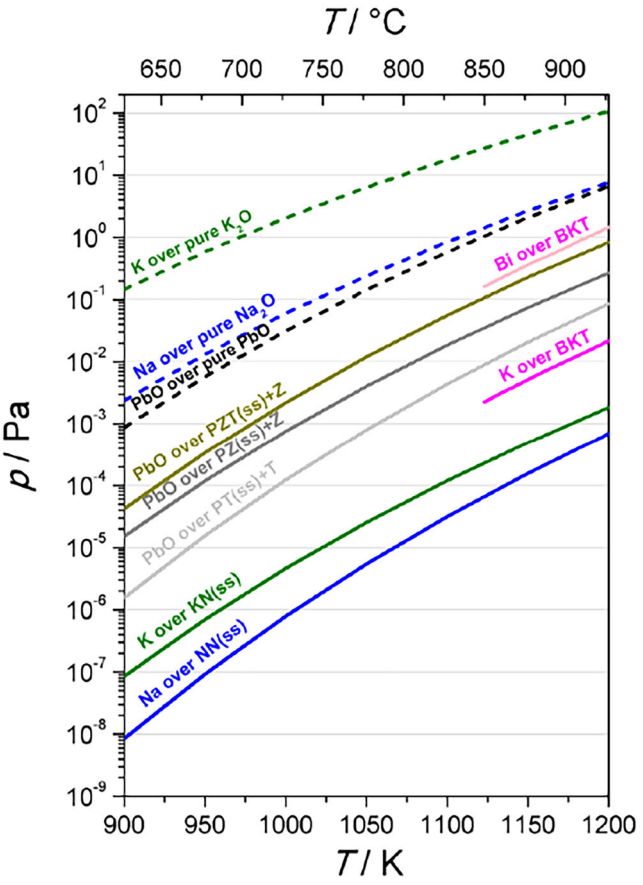

FIGURE 3 Equilibrium vapor pressures and their temperature dependences data for various volatile oxides.[66]

Li-modified (Na,K)NbO_3:($Li_{0.06}Na_{0.52}K_{0.42}$)$NbO_3$ resulted in the electrically and mechanically hardening, which was considered as being the result of the volatilization of A-site alkali metals species such as Li_2O, K_2O, and Na_2O. In this case, V_A' was partially replaced with the excessive amount of Li^+ that came from the Li_2SiO_7 glass phase formed with Li_2CO_3 and SiO_2 sintering aids. Although it is difficult to analyze the volatilization amount quantitatively and is still controversial in some papers,[69–71] it is noteworthy that the alkali volatilization has a depth profile as reported elsewhere.[68,72] As seen in Figure 4, the Curie temperature of the intentionally annealed Li-modified (Na,K)NbO_3 came back to the as-sintered value after the polish off about 75 μm from both sides of the disk sample. This depth profile will be beneficial for multilayered piezoceramics in terms of the design flexibility of the piezo-active area from the surface shown in Figure 5A,F.[73]

All the same, base $NaNbO_3$ and (Na,K)NbO_3 without a flux or liquid phase additive are still difficult to sinter to high densities in air, but they can be sintered in low partial pressures of oxygen.[66,67,74–78] As an example, the sintering of $NaNbO_3$ in air and under reducing conditions can greatly impact density, microstructure, and dielectric and piezoelectric properties. Details of the experimental methods are found in Shimizu et al.[78]

From the observations in Figure 6, we noted that sintering under low partial pressures of oxygen (p_{O_2} ~10^{-10} atm at peak temperatures between 1240°C and 1275°C) results in higher relative densities of $NaNbO_3$ than sintering the same powders in air between 1250°C and 1325°C. The microstructure also shows high residual pores in the lower density with air-fired $NaNbO_3$ ceramics.

Although the focus of this paper is mostly regarding the non-stoichiometry of important dielectric and piezoelectric materials, other reviews cover these comparisons concerning microstructure differences. There are essential connections between the non-stoichiometry and the microstructure evolution and this is discussed in part. For further details, we recommend a review by Malič et al. Here, it is pointed out that for alkali niobate materials the nature of the densification and microstructure evolution are an important feature of this family of materials that is impacted with the sintering atmosphere.[66] Alkali niobate ceramics sintered in air have limited densification with a high level of porosity. This issue is linked to rapid grain growth in the early stage of sintering, which leads to a skeletal microstructure for the air sintering case. As noted by Fisher et al., the sintering atmosphere can impact both the densification and grain boundary morphologies and provide a means to control of the densification and grain shape.[79] In the case of $BaTiO_3$, Jung et al. showed a reduction in the grain boundary roughness when sintered at low oxygen partial pressures.[80] This phenomenon suppresses the rapid grain growth and therefore balances the densification and grain growth kinetics such that higher densities and more uniform grain structures occur. The observations are known but the complex relationships between the sample surface non-stoichiometry, liquid-phase sintering aids, and the surface stoichiometry of the grain boundary are still only qualitatively connected through structure–property–process relations and require further research.

Despite the fact that the volatility and the partial pressures are lower in the $NaNbO_3$ than the PZT ceramics, these materials are very sensitive to the sintering process. In sintering at lower partial pressures, the concentration of oxygen vacancy and metal vacancy can be suppressed, as we noted in PZT. After sintering at low p_{O_2}, we can re-oxidize with a thermal annealing in oxidizing atmosphere with partial pressures ranging from $p_{O_2} \sim 10^{-6}$ atm and above. This enhances the resistivity and improves the dielectric losses, and the high-field ferroelectric and piezoelectric properties. Figure 7 shows the difference between the polarization and strain hysteresis of the $NaNbO_3$ sintered in the low partial pressures and air atmospheres,

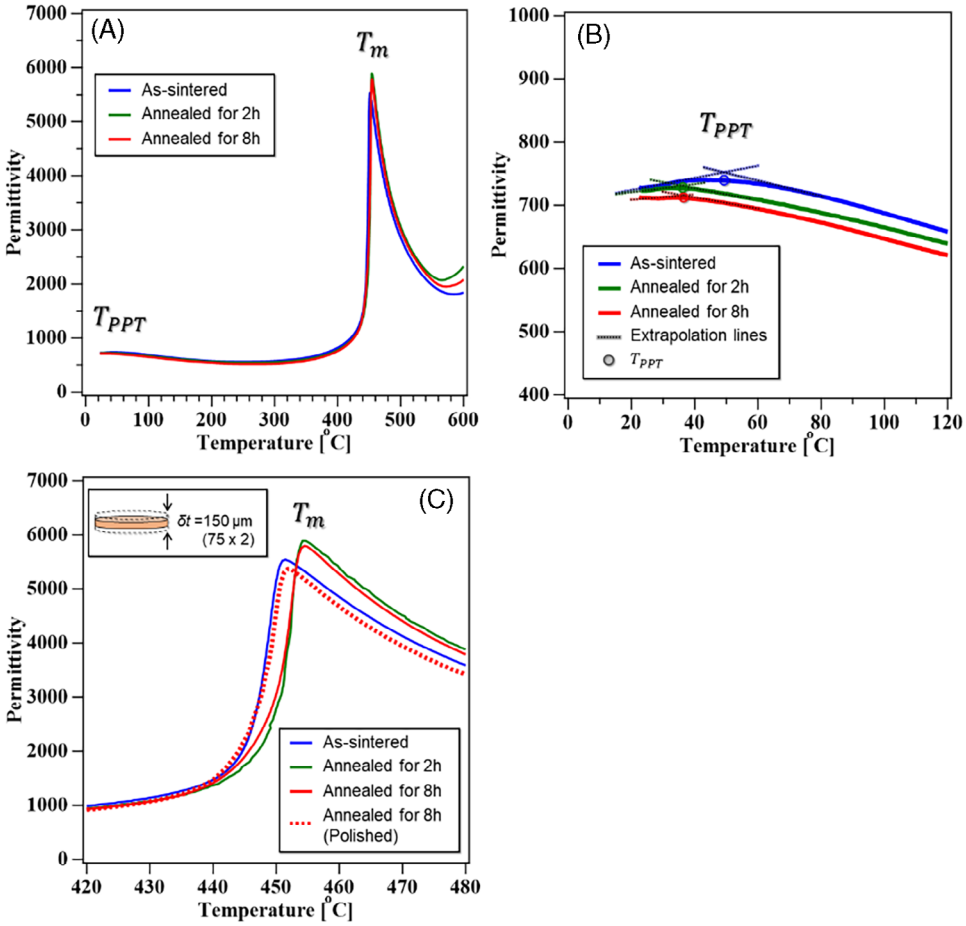

FIGURE 4 (A) Temperature-dependent permittivity change of the post-annealed (Li,Na,K)NbO_3 piezoceramics. (B) The magnified view of the permittivity changes around polymorphic phase transition temperature T_{PPT}. (C) The temperature at the maximum permittivity T_m as the phase transition from tetragonal to cubic is indicated. In addition to the post-annealing dependence of the permittivity, the result for 8 h annealed sample, which was polished by 75 μm from both side of the surface is shown.[68]

with the superior properties being associated with the low partial pressure cases.

It is important to note that $NaNbO_3$ is a material that has a degenerate phase mixing of a ferroelectric and antiferroelectric phase, sometimes known as P and Q phases, respectively. The P phase is the antiferroelectric phase with a space group symmetry (*Pbma*) and the Q phase has a space group ($P2_1ma$) that coexist in the undoped cases. We do not observe the double hysteresis associated with the antiferroelectric phase as the applied field transitions the antiferroelectric P phase into the ferroelectric phase, and there is no back switching to the antiferroelectric phase, so we observe the ferroelectric square hysteresis loop. Forming solid solutions and lowering the so-called Goldschmidt tolerance factor has proven to be an effective strategy to develop antiferroelectric behavior and eliminate the ferroelectric. Details of these solid solutions are discussed elsewhere.[81–83] The important point to note here is we observe higher remanent polarization in the low p_{O_2} sintered atmospheres than in air-fired materials. Likewise, the electromechanical strain and the applied electric field hysteresis show so-called butterfly loops, with higher strains in the low p_{O_2} sintered atmospheres relative to the air-fired $NaNbO_3$ ceramics.

2.3 | $(Bi_{0.5}Na_{0.5})TiO_3$ and $(Bi_{0.5}Na_{0.5})TiO_3$–$BaTiO_3$ cases

These perovskite compositions, which are based on $(Bi_{0.5}Na_{0.5})TiO_3$ and $(Bi_{0.5}Na_{0.5})TiO_3$–$BaTiO_3$ are also of interest as lead-free piezoelectric materials and possible dielectrics for capacitors.[84–86] In the $(Bi_{0.5-x}Na_{0.5})TiO_3$, Bi-deficient stoichiometries have shown remarkably high ionic conduction for the oxygen vacancies.[87–89] So, for these series of materials, the piezoelectric and dielectric applications will require close attention to the potential electromigration of the oxygen vacancy that can lead to time-dependent breakdown under direct current bias fields in the applications. This means that the volatility

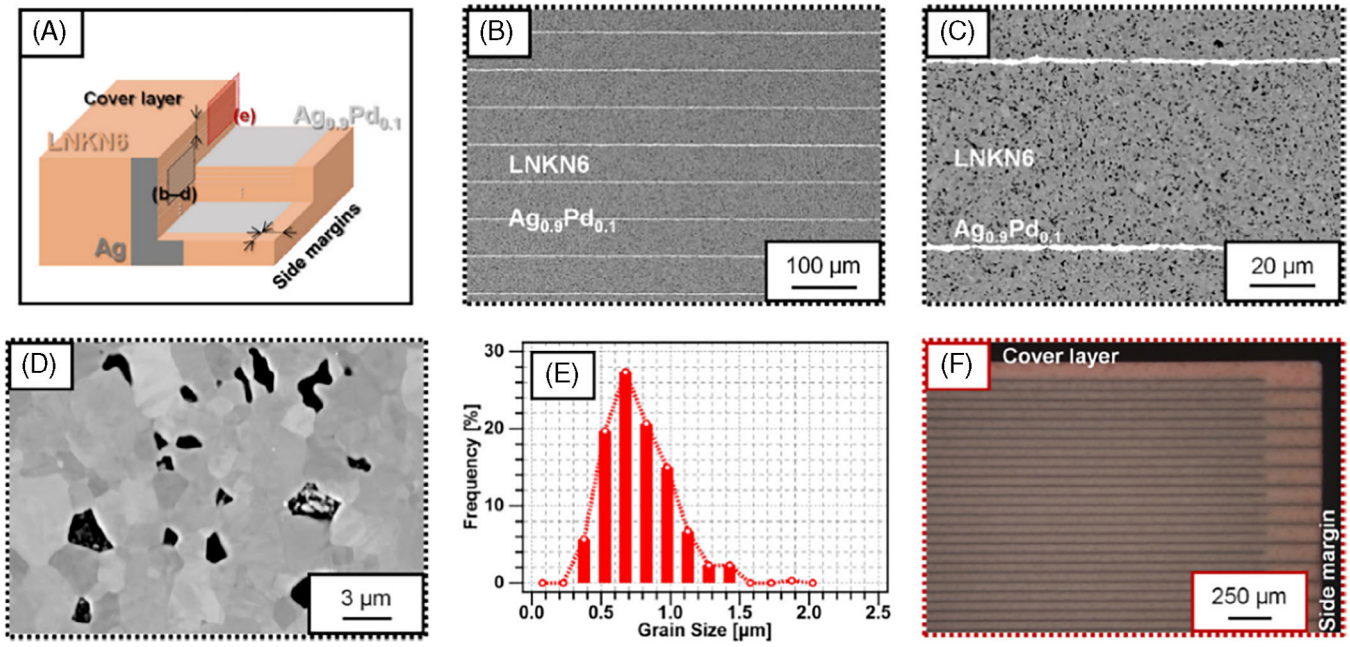

FIGURE 5 (A) Schematic illustration of the multilayered structure of $(Li,Na,K)NbO_3$ with Ag/Pd inner electrode. Observation area of scanning electron microscopy (SEM) (B–D) and digital microscope (E) is shown. (B and C) Secondary-electron images of a cross-sectional plane of the multilayer measured by the SEM. (D) Grain structure on the piezoelectric layer of the multilayer using a backscattering emission image. (E) Grain size distribution on the sample surface. (F) Dark-field image of the edge of the multilayer actuator obtained with the digital microscope. Reprinted with permission. Copyright 2022 AIP Publishing.[73]

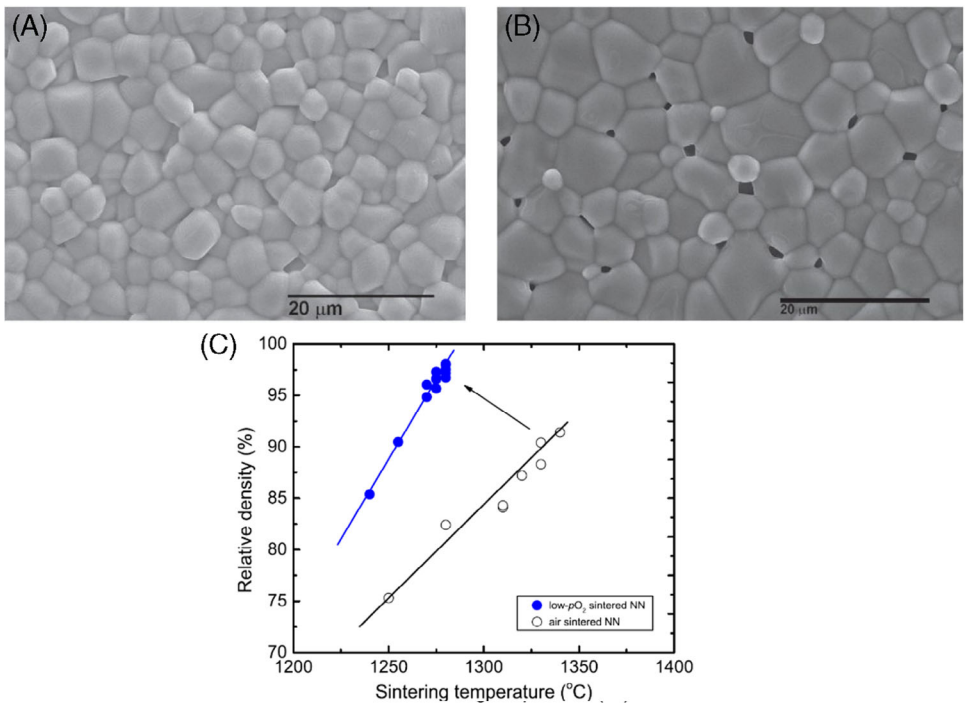

FIGURE 6 Scanning electron microscopy of a thermally annealed surface to determine the microstructure of $NaNbO_3$ sintering at a low partial pressure of (A) oxygen (p_{O_2} ~10^{-10} atm) and (B) in air atmospheres. (C) Comparison of the relative densities of $NaNbO_3$ ceramics sintered at different temperatures under low partial pressures and air atmospheres. Reprinted with permission. Copyright 2014 John Wiley and Sons.[78]

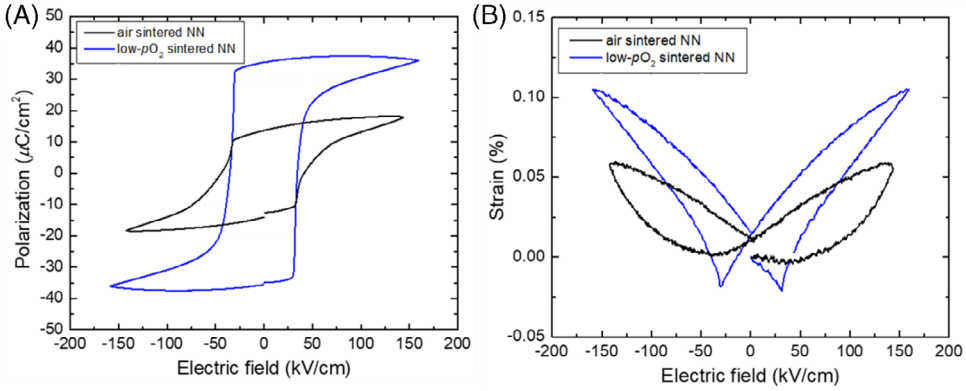

FIGURE 7 Comparison of the (A) polarization–electric field and (B) strain–electric field hysteresis loops of the $NaNbO_3$ sintered in air and low p_{O_2} atmospheres. Reprinted with permission. Copyright 2014 John Wiley and Sons.[78]

of the Bi and O species in the sintering process is also an important consideration. For example, Figure 3 shows that the higher vapor pressure is associated with the Bi relative to the K volatility for $(Bi_{0.5}K_{0.5})TiO_3$, and the Bi volatility is on the scale of the lead volatility of the PZT materials. In the $(Bi_{0.5}Na_{0.5})TiO_3$–$BaTiO_3$, we have demonstrated that Bi_2O_3 excess and quenching in the final stages of sintering impact the defects and the associated ferroelectric properties.[90,91] The excess Bi_2O_3 oxide content, the calcination temperature, the final sintering temperatures and time are all sensitive to varying the point defect content, microstructure, and ferroelectric properties.

Note that, in the $(Bi_{0.5}Na_{0.5})TiO_3$ system, non-stoichiometric compositions such as with A-poor or B-rich compositions lead to grain growth,[92–95] which is in contrast to that of PZT[96] and $(Na,K)NbO_3$[97] systems. Also grain growth is suppressed in PZT[41] and $(Na,K)NbO_3$[76,79,98] under reduced atmosphere, whereas the $(Bi_{0.5}Na_{0.5})TiO_3$ system shows a slight grain growth.[99] The rationale for these differences is not well understood at this time. From a stoichiometry–property perspective, it is also noted that the non-stoichiometry controlled and sintering atmospheres affect some important physical properties such as the ionic conductivity and the depolarization temperature T_d. In the articles of both Seo et al. and Qiao et al., there is a higher T_d with the Bi-deficient composition BNT-6BT.[92,95] Although these trends are explained with only oxygen vacancies, this is not completely proven. A greater non-stoichiometry that drives an exsolution reaction results in high BT (BNT-BT) as will be shown later.

The Bi_2O_3 volatility reaction in the $(Bi_{0.5}Na_{0.5})TiO_3$ system is given by:

$$2Bi_{Bi}^{\times} + 3O_O^{\times} \rightarrow 2V_{Bi}^{'''} + 3V_O^{\cdot\cdot} + Bi_2O_3 \uparrow \qquad (12)$$

At high sintering temperatures, this leads to an ionically compensated condition. Similar to the PZT case, there can also be an oxygen uptake from the air atmosphere in the furnace and this compensates with an electronic hole compensation. So, with loss of Bi and O species, we would expect an increase in ionic conductivity. A surprising and informative example is sintering times of a batched Bi-deficient by 1.2% for $0.85(Bi_{0.5}Na_{0.5})TiO_3$−$0.15BaTiO_3$ compositions.[100] These are then sintered for different times at a temperature of 1200°C with 5°C/min heating and cooling rates. The sintering hold times vary between 20, 120, and 600 min. Through impedance measurement there are orders of magnitude differences over the different sintering times, with the real component of impedance increasing with time. That is at first sight a very surprising observation as this means that the conductivity is decreasing. Figure 8 shows electrical characteristics with impedance in the highly Bi-deficient densified materials, and these are also compared to a stoichiometrically batched composition. We note that the stoichiometric batching will have some impact from the volatility but not at the concentration levels of the deficient batched case. The effect is large and we noted that the 20- and 120-min sintering times of the $0.85(Bi_{0.5}Na_{0.5})TiO_3$−$0.15BaTiO_3$ Bi-deficient are having very small levels of resistances due to the high ionic conduction. By the time the sintering hold time is 600 min, the impedance almost matches the stoichiometrically batch samples, which indicates that there has been a re-equilibration of the defect chemistry that controls the conductivity of the material. This would imply that the change is reducing the concentration of Bi vacancies and compensating oxygen vacancies.

As mentioned above, a dielectric property parameter impacted by Bi_2O_3 loss is the depolarization temperature, T_d. This T_d is the phase boundary between the

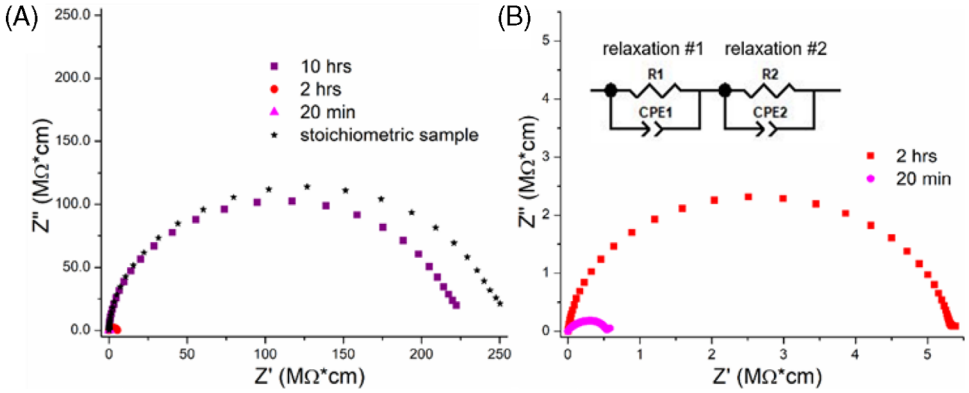

FIGURE 8 (a and b) Impedance from sintering temperature of 1200°C as function of sintering time for different holds between 20 min, 2 h, and 10 h for a Bi-deficient $0.85(Bi_{0.5}Na_{0.5})TiO_3{-}0.15BaTiO_3$. Real part of the impedance increasing with longer times and after 10 h and approaches the impedance of a shorter time stoichiometrically sintered ceramic. Reprinted with permission. Copyright 2023 John Wiley and Sons.[100]

low-temperature normal ferroelectric phase and the relaxor ferroelectric phase and gives a dielectric anomaly at the T_d. The normal ferroelectric phase has a tetragonal symmetry of $P4mm$, and at T_d, there is a transition to a pseudocubic symmetry. For this case, the T_d is sensitive to various parameters such as drops with sintering time in the 1.2% Bi-deficient solid solution, from ~236°C in 20 min to ~226°C in 120 min to ~210°C in 600 min. Note that, the cooling rate from the sintering temperature was always 5°C/min; therefore, it can be ruled out thermal stress effect onto T_d.[101,102] Additionally, the stoichiometric $0.85(Bi_{0.5}Na_{0.5})TiO_3{-}0.15BaTiO_3$ is exactly 210°C.[103] Taking into consideration that $[V_O^{\cdot\cdot}]$ tends to stabilize the polar nano-regions resulting in the increase in T_d,[92,95] the observed decrease in T_d during the holding time at sintering process should also be corresponded to the decrease in the amount of $[V_O^{\cdot\cdot}]$.

From a transmission electron microscopy study, it is found that there is a secondary phase that continues to increase with the sintering hold time, and this is the formation of a $BaTi_2O_5$ phase (Figure 9A). This suggests that in the sintering process, we exceed the non-stoichiometric defect concentrations within this solid solution. So, an exsolution reaction occurs in the sintering of this solid solution, and the non-stoichiometry changes as we lose Bi and O in accordance with Equation (12), and when it exceeds a critical concentration of defects in the solid solution, X_c (Equation 14).

The deficient non-stoichiometric solid solution is given by $y = 0.15$ for the case in-hand:

$$(1-y)\left(Na_{0.5}Bi_{0.5-x}\square_x\right)TiO_{3-1.5x}\square_{1.5x} - yBaTiO_3 \quad (13)$$

When $x \sim x$, it is not in equilibrium, so it drives the following exsolution reaction of the solid solution and it changes the composition of the perovskite phase and forms a secondary phase:

$$(1-y)\left(Na_{0.5}Bi_{0.5-x_c}\square_{x_c}\right)TiO_{3-1.5x_c}\square_{1.5x_c} - yBaTiO_3 \rightarrow \left\{(1-y)\left(Na_{0.5}Bi_{0.5-x_c}\square_{x_c-\delta/(1-y)}Ba_{\delta/(1-y)}\right)TiO_{3-1.5x_c}\square_{1.5x_c-\delta/(1-y)} - (y-2\delta)\,BaTiO_3\right\} + \delta BaTi_2O_5 \quad (14)$$

The formation of the secondary phase, $BaTi_2O_5$ effectively reduces the Ti content and partially increases the Ba content in the perovskite phase. With the exsolution reaction creating a renormalization of the composition, and this will have an impact on the ferroelectric properties from the starting composition with 15 mol% $BaTiO_3$.

On reducing the $BaTiO_3$ mol% from 15%, there is initially a monotonic decrease in the T_d, and as it approaches the morphotropic phase boundary at ~10 mol% $BaTiO_3$ there is an asymptotic reduction in T_d, as indicated in Figure 9B. On the basis of the renormalization of the $BaTiO_3$ after the 10-h sintering time, the exsolution is equivalent to approximately $0.88(Bi_{0.5}Na_{0.5})TiO_3{-}0.12BaTiO_3$ with the $BaTi_2O_5$ second-phase formation, the $\delta \sim 0.015$ in considering Equation (15).

As covered in earlier studies, the donor and acceptor doping can also impact the manner in which the $0.85(Bi_{0.5}Na_{0.5})TiO_3{-}0.15BaTiO_3$ compensates for different atmospheres with sintering and secondary annealing.[103,105] It is clear that there are a number of degrees of freedom in which the $(Bi_{0.5}Na_{0.5})TiO_3{-}BaTiO_3$ system compensates the non-stoichiometry and each scenario has to be carefully considered with systematic variation of dopants, Bi_2O_3 excess and deficient composition, atmosphere, and sintering temperatures.

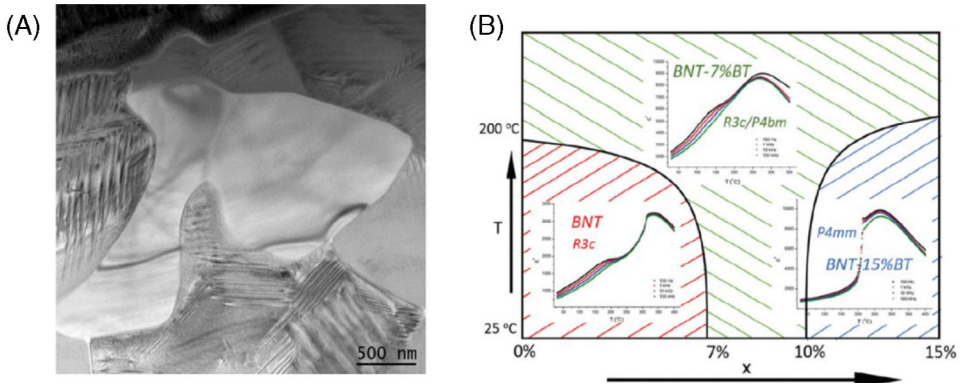

FIGURE 9 (A) Transmission electron microscopy (TEM) image of the 600 min sintering hold time with the growth of the $BaTi_2O_5$ phase with the exsolution decomposition of the Bi-deficient $0.85(Bi_{0.5}Na_{0.5})TiO_3-0.15BaTiO_3$. Reprinted with permission. Copyright 2023 John Wiley and Sons.[100] (B) The phase diagram of the $(Bi_{0.5}Na_{0.5})TiO_3$–$BaTiO_3$ ferroelectric phases with temperature as a function of $BaTiO_3$. Reprinted with permission. Copyright 2021 John Wiley and Sons.[104]

2.4 | Mn doping of dielectrics and compensation: $Ca(Hf,Ti,Mn)O_3$

Manganese is one of the most well-known dopants because it effectively suppresses the conductivity of electroceramics. Despite of its popularity, the mechanism how Mn suppress the conductivity from the view point of the multivalence metal is often overlooked. In this review, where the example of A-site volatility and redox reactions with oxygen was a dominant focus, we also wish to remind the reader that the doping with multivalence metal for dielectric and piezoelectric materials is also an important factor in different sintering and cooling atmospheres. $Ca(Hf,Ti,Mn)O_3$ dielectric material is gathering a lot of interest as a class I capacitors that can operate at high temperatures and under high electric fields for power electronic applications.[106–108]

Manganese is a classical compositional additive that can be added into dielectric formulations that aids in increasing the resistivity and improving reliability. The valence of Mn is very sensitive to temperature and oxygen partial pressures, as shown in Figure 10A.[109,111] Manganese is a multivalent ion depending on oxygen partial pressure and temperature, with Mn^{3+} and Mn^{4+} being in the expected valence states when fired in air.[112–114] The defect reactions for the oxidation of Mn^{2+}, Mn^{3+}, and Mn^{4+} are as follows:

$$2Mn''_{Mn} + 2V_O^{\cdot\cdot} + \frac{1}{2}O_2 \rightarrow 2Mn'_{Mn} + V_O^{\cdot\cdot} + O_O^{\times} \quad (15)$$

$$2Mn'_{Mn} + V_O^{\cdot\cdot} + \frac{1}{2}O_2 \rightarrow 2Mn_{Mn}^{\times} + O_O^{\times} \quad (16)$$

Upon cooling to room temperature, the Mn is expected to be transitioned to Mn^{4+} if it is sintered in oxidizing conditions. The concentration of compensating oxygen vacancies that resulted from Mn^{3+} at high temperatures will then minimized, thus reducing the ionic conductivity in $Ca(Ti_{0.795}Mn_{0.005}Hf_{0.2})O_3$, as shown in Figure 10B.[115]

In air sintering composition with $Ca(Ti_{0.8}Hf_{0.2})O_3$ and $Ca(Ti_{0.795}Mn_{0.005}Hf_{0.2})O_3$, there is a large difference in the impedance Cole–Cole plots, which is due to the Mn oxidation suppressing the ionic conduction. There are two major relaxations: the first relaxation corresponds to the sum of ionic and electronic, and the second relaxation is related to the blocking of the oxygen vacancies at the electrode to provide an ionic polarization that is represented by a ceramic–electrode interface. We can see that the impedance spectra of Mn-doped sample have suppressed the ionic relaxation to just the single relaxation, and this is controlled by the electronic conductivity and the capacitance. With the higher resistivity with the Mn doping and this limits the high field losses and provides higher breakdown strength with greater temperature stability, as shown in Figure 11. Characteristic breakdown strengths were also obtained using Weibull statistics, in which the breakdown strengths are ranked in increasing order and the median rank (MR) of the data is calculated as:

$$\mathrm{MR} = \frac{j - 0.3}{N + 0.4}$$

where j is the rank and N is the total number of samples. The characteristic breakdown strength is then determined from the zero–intercept of $\ln(E)$ versus $\ln[\ln\{1/(1 - \mathrm{MR})\}]$, as shown in Figure 12. The Weibull modulus, which determines the degree of variation in the data set, is determined from the slope of the linear trend line. From this data, the difference in temperature dependence between the two materials and the high-voltage–high-temperature benefits associated with Mn doping in this system can clearly be seen.

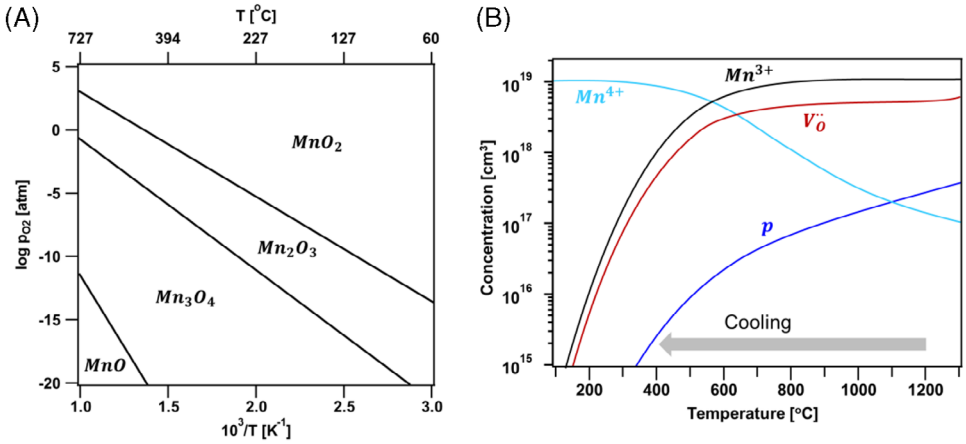

FIGURE 10 (A) Manganese oxide phases as a function of partial pressure and temperature. Reprinted with permission. Copyright 2005 John Wiley and Sons.[109] (B) Schematic of the Mn multivalent states bases on thermodynamic constants in Mn-doped perovskites (assuming similar constants to $SrTiO_3$).[110]

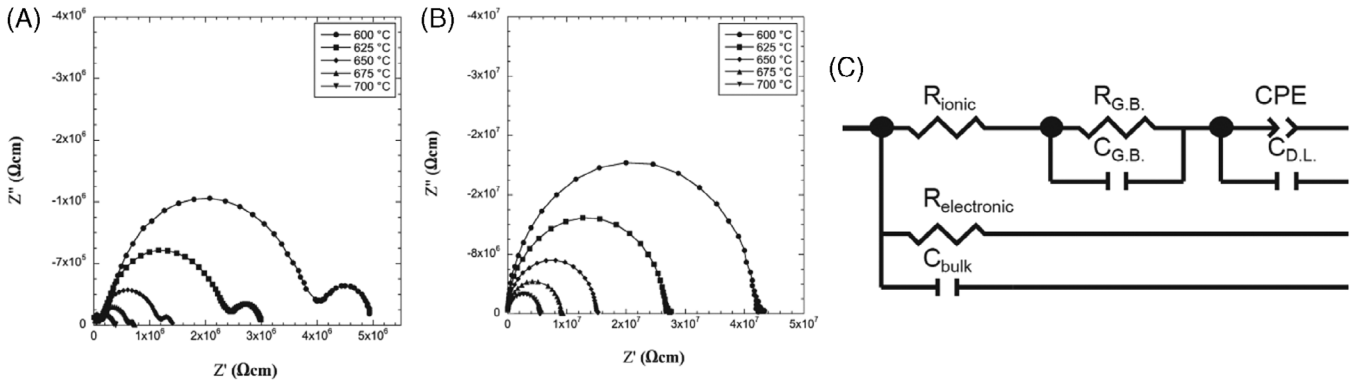

FIGURE 11 Impedance spectra plotted in the form of Cole–Cole plots from 600°C to 700°C for (A) $Ca(Ti_{0.8}Hf_{0.2})O_3$ and (B) $Ca(Ti_{0.795}Mn_{0.005}Hf_{0.2})O_3$, and (C) an equivalent circuit for the impedance response with mixed ionic and electronic conduction. Reprinted with permission. Copyright 2011 John Wiley and Sons.[115]

3 | SUMMARY AND PERSPECTIVES

This paper provides a number of examples of the importance of understanding relationship between the atmosphere used in the thermal processing of dielectric-based functional ceramics and the defects and their compensation mechanisms to create non-stoichiometric compositions. In particular, in the cases discussed we largely focused on compositions that can be volatile with high vapor pressures, such cases are of particular importance in Pb, Bi, and alkali metal-based piezoelectric ceramics materials. The volatilization can also be impacted by lowering the partial pressure of oxygen at the sintering atmosphere, which can slow the metal cation volatilization, but increase the overall oxygen vacancy concentration; therefore, a lower temperature re-oxidation step is needed to limit these concentrations. The cooling in a furnace can also lead to a transition from an ionically compensated defect concentration with the loss of the cations and oxygen, and then on cooling in an air atmosphere there is an uptake of oxygen through the re-oxidation reaction, which can lead to an electronic compensation of the metal vacancies that are created at the higher sintering temperature. The rate of this transition and change in compensation depend on the atmosphere, the cooling rate, and the size of the components.

In materials such as $NaNbO_3$ and $(Na,K)NbO_3$ there are advantages in the sintering at low partial pressures, with better control of the densification, grain size, and electrical properties with sintering at lower partial pressures and then re-oxidizing at higher p_{O_2} at lower temperatures. Note that, even in the case of air firing, the multilayered structure with protecting layers enclosing piezo-active layers with a certain margin of about 75 μm can rule out the effect of the alkali volatilization effect.

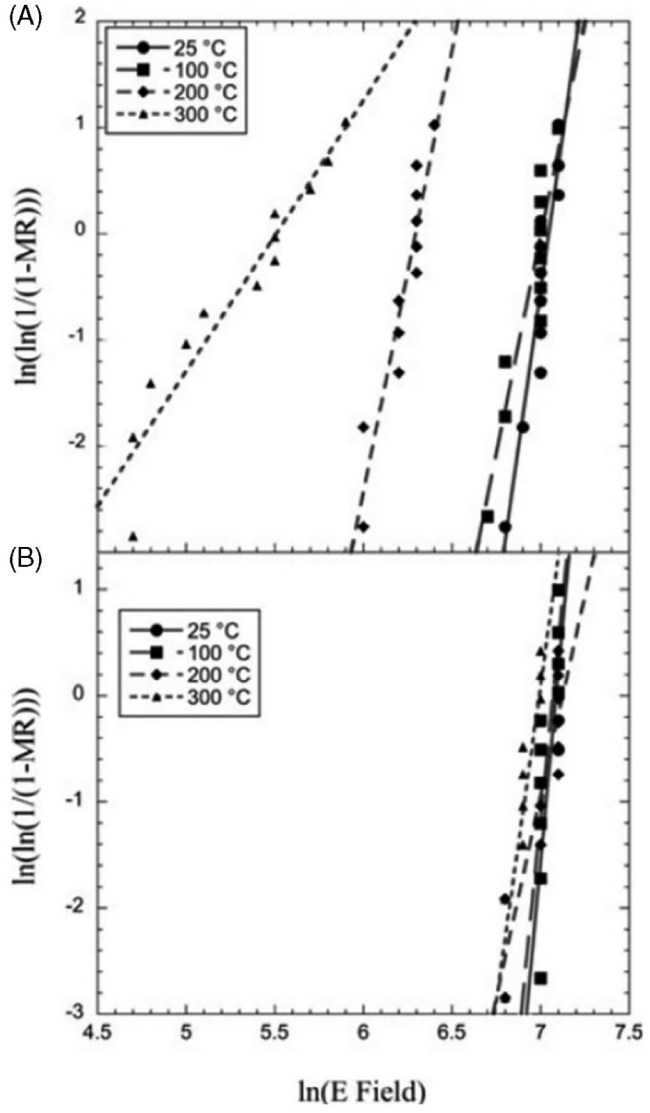

FIGURE 12 Comparison of the Weibull plots of electrical breakdown strength in (A) $Ca(Ti_{0.8}Hf_{0.2})O_3$ and (B) $Ca(Ti_{0.795}Mn_{0.005}Hf_{0.2})O_3$. Reprinted with permission. Copyright 2011 John Wiley and Sons.[115]

The defect chemistry of $(Bi_{0.5}Na_{0.5})TiO_3$–$BaTiO_3$ is very complex with many degrees of freedom controlling the non-stoichiometry. Here, we demonstrated that if we batch the initial chemistry with Bi deficiency and then with extended sintering times, the impedance increased contrary to the expected cases, which should increase with the Bi and O losses. The reason for this observation is that there is an exsolution reaction with a secondary phase formation of $BaTi_2O_5$, which effectively increase the Ba content to partially compensate for the unstable V''_{Bi} concentrations. Finally, we also considered an example of Mn doping in a linear dielectric. In particular, the advantage of Mn doping is having sufficient time to re-oxidize the multivalent states to a neutral $Mn^{\times}_{Mn}$ by re-oxidation and minimizing the oxygen vacancy concentration.

All in all, there are many other aspects of controlling the defect chemistry of a given material, but the examples given here illustrate the importance of thinking through the basic material composition and its impact on the sintering process. It is hoped that with these insights, researchers will have a better understanding of the processing–property relations in functional ceramics.

ACKNOWLEDGMENTS

This work was based on several research efforts that were sponsored through the National Science Foundation, as part of the Center for Dielectrics and Piezoelectrics under grant nos. IIP-1841453 and 1841466.

ORCID

Clive A. Randall https://orcid.org/0000-0002-5478-2699
Hiroshi Nishiyama https://orcid.org/0000-0002-9670-0575
Hiroyuki Shimizu https://orcid.org/0000-0002-3680-5690

REFERENCES

1. Trolier-Mckinstry S, Zhang S, Bell AJ, Tan X. High-performance piezoelectric crystals, ceramics, and films. Annu Rev Mater Res. 2018;48:191–217. https://doi.org/10.1146/annurev-matsci-070616-124023
2. Shibata K, Oka F, Ohishi A, Mishima T, Kanno I. Piezoelectric properties of (K,Na)NbO_3 films deposited by RF magnetron sputtering. Appl Phys Express. 2008;1:011501. https://doi.org/10.1143/APEX.1.011501
3. Hennings DFK. Dielectric materials for sintering in reducing atmospheres. J Eur Ceram Soc. 2001;21:1637–42. https://doi.org/10.1016/S0955-2219(01)00082-6
4. Kunihiro Nagata KN. Properties of piezoelectric ceramics sintered in reducing atmosphere. Jpn J Appl Phys. 1991;30(9B):2224–27. https://doi.org/10.1143/JJAP.30.2224
5. Randall CA, Kim N, Kucera J-P, Cao W, Shrout TR. Intrinsic and extrinsic size effects in fine-grained morphotropic-phase-boundary lead zirconate titanate ceramics. J Am Ceram Soc. 1998;81(3):677–88. https://doi.org/10.1111/j.1151-2916.1998.tb02389.x
6. Okazaki K. Developments in fabrication of piezoelectric ceramics. Ferroelectrics. 1982;41:77–96. https://doi.org/10.1080/00150198208210611
7. Tuller HL, Bishop SR. Point defects in oxides: tailoring materials through defect engineering. Annu Rev Mater Res. 2011;41:369–98. https://doi.org/10.1146/annurev-matsci-062910-100442
8. Duncan KL, Wachsman ED. General model for the functional dependence of defect concentration on oxygen potential in mixed conducting oxides. Ionics (Kiel). 2007;13:127–40. https://doi.org/10.1007/s11581-007-0087-x
9. Randall CA, Yousefian P. Fundamentals and practical dielectric implications of stoichiometry and chemical design in a high-performance ferroelectric oxide: $BaTiO_3$. J Eur Ceram Soc. 2022;42:1445–73. https://doi.org/10.1016/j.jeurceramsoc.2021.12.007

10. Maier J. Defect chemistry: composition, transport, and reactions in the solid state. Part I: thermodynamics. Angew Chem Int Ed Eng. 1993;32(3):313–35. https://doi.org/10.1002/anie.199303133
11. Smith DM. The defect chemistry of metal oxides. Oxford, England: Oxford University Press; 2000.
12. Barsoum MW. Fundamentals of ceramics. Boca Raton, FL: CRC Press; 2019.
13. Atkin RB, Fulrath RM. Point defects and sintering of lead zirconate-titanate. J Am Ceram Soc. 1971;54(5):265–70. https://doi.org/10.1111/j.1151-2916.1971.tb12286.x
14. Lemke F, Rheinheimer W, Hoffmann MJ. Sintering and grain growth in $SrTiO_3$: impact of defects on kinetics. J Ceram Soc Japan. 2016;124(4):346–53. https://doi.org/10.2109/jcersj2.15265
15. Ferreira SO. Advanced topics in crystal growth. London, UK: IntechOpen; 2013.
16. Sossi PA, Fegley B. Thermodynamics of element volatility and its application to planetary processes. Rev Miner Geochem. 2018;84:393–459. https://doi.org/10.2138/rmg.2018.84.11
17. Boukamp B, Pham M, Blank D, Bouwmeester H. Ionic and electronic conductivity in lead–zirconate–titanate (PZT). Solid State Ionics. 2004;170:239–54. https://doi.org/10.1016/j.ssi.2004.03.005
18. Jamnik J, Maier J. Generalised equivalent circuits for mass and charge transport: chemical capacitance and its implications. Phys Chem Phys. 2001;3:1668–78. https://doi.org/10.1039/B100180I
19. Jamnik J, Maier J. Treatment of the impedance of mixed conductors equivalent circuit model and explicit approximate solutions. J Electrochem Soc. 1999;146(11):4183–88. https://doi.org/10.1149/1.1392611
20. Lai W, Haile SM. Impedance spectroscopy as a tool for chemical and electrochemical analysis of mixed conductors: a case study of ceria. J Am Ceram Soc. 2005;88(11):2979–97. https://doi.org/10.1111/j.1551-2916.2005.00740.x
21. Waser R, Baiatu T, Härdtl K-H. dc electrical degradation of perovskite-type titanates: I, ceramics. J Am Chem Soc. 1990;73(6):1645–53. https://doi.org/10.1111/j.1151-2916.1990.tb09809.x
22. Yang GY, Lian GD, Dickey EC, Randall CA, Barber DE, Pinceloup P, et al. Oxygen nonstoichiometry and dielectric evolution of $BaTiO_3$. Part II: insulation resistance degradation under applied dc bias. J Appl Phys. 2004;96(12):7500–7508. https://doi.org/10.1063/1.1809268
23. Randall CA, Kelnberger A, Yang GY, Eitel RE, Shrout TR. High strain piezoelectric multilayer actuators—a material science and engineering challenge. J Electroceram. 2005;14:177–91. https://doi.org/10.1007/s10832-005-0956-5
24. Koh J-H, Jeong S-J, Ha M-S, Song J-S. Degradation and cracking behavior of $0.2(PbMg_{1/3}Nb_{2/3}O_3)$–$0.8(PbZr_{0.475}Ti_{0.525}O_3)$ multilayer ceramic actuators. Sens Actuators A. 2004;112:232–36. https://doi.org/10.1016/j.sna.2004.01.001
25. Frömling T, Schintlmeister A, Hutter H, Fleig J. Oxide ion transport in donor-doped $Pb(Zr_xTi_{1-x})O_3$: the role of grain boundaries. J Am Ceram Soc. 2011;94(4):1173–81. https://doi.org/10.1111/j.1551-2916.2010.04158.x
26. Rahmati B, Fleig J, Sigle W, Bischoff E, Maier J, Rühle M. Oxidation of reduced polycrystalline Nb-doped $SrTiO_3$: characterization of surface islands. Surf Sci. 2005;595:115–26. https://doi.org/10.1016/j.susc.2005.07.041
27. Ren X. Large electric-field-induced strain in ferroelectric crystals by point-defect-mediated reversible domain switching. Nat Mater. 2004;3(2):91–94. https://doi.org/10.1038/nmat1051
28. Matsuo H, Utsunomiya M, Noguchi Y. Utilizing ferrorestorable polarization in energy-storage ceramic capacitors. NPG Asia Mater. 2022;14(80):1–9. https://doi.org/10.1038/s41427-022-00426-z
29. Ichikawa Y, Kitanaka Y, Oguchi T, Noguchi Y, Miyayama M. Polarization degradation and oxygen-vacancy rearrangement in Mn-doped $BaTiO_3$ ferroelectrics ceramics. J Ceram Soc Jpn. 2014;122(6):373–80. https://doi.org/10.2109/jcersj2.122.373
30. Eichel R-A, Kungl H, Jakes P. Defect structure of non-stoichiometric and aliovalently doped perovskite oxides. Mater Technol. 2013;28(5):241–46. https://doi.org/10.1179/175355513X13715615193120
31. Genenko YA, Glaum J, Hoffmann MJ, Albe K. Mechanisms of aging and fatigue in ferroelectrics. Mater Sci Eng B. 2015;192(C):52–82. https://doi.org/10.1016/j.mseb.2014.10.003
32. Glaum J, Hoffman M. Electric fatigue of lead-free piezoelectric materials. J Am Ceram Soc. 2014;97(3):665–80. https://doi.org/10.1111/jace.12811
33. Fan Z, Tan X. In-situ TEM study of the aging micromechanisms in a $BaTiO_3$-based lead-free piezoelectric ceramic. J Eur Ceram Soc. 2018;38:3472–77. https://doi.org/10.1016/j.jeurceramsoc.2018.03.049
34. Maier RA, Pomorski TA, Lenahan PM, Randall CA. Acceptor-oxygen vacancy defect dipoles and fully coordinated defect centers in a ferroelectric perovskite lattice: electron paramagnetic resonance analysis of Mn^{2+} in single crystal $BaTiO_3$. J Appl Phys. 2015;118:164102. https://doi.org/10.1063/1.4934505
35. Maier RA, Randall CA. Low-temperature ionic conductivity of an acceptor-doped perovskite: I. Impedance of single-crystal $SrTiO_3$. J Am Ceram Soc. 2016;99(10):3350–59. https://doi.org/10.1111/jace.14348
36. Chandrasekaran A, Damjanovic D, Setter N, Marzari N. Defect ordering and defect-domain-wall interactions in $PbTiO_3$: a first-principles study. Phys Rev B—Condens Matter Mater Phys. 2013;88(21):214116. https://doi.org/10.1103/PhysRevB.88.214116
37. Morozov MI, Einarsrud M-A, Tolchard JR, Geiger PT, Webber KG, Damjanovic D, et al. In-situ structural investigations of ferroelasticity in soft and hard rhombohedral and tetragonal PZT. J Appl Phys. 2015;118:164104. https://doi.org/10.1063/1.4934615
38. Waser R. Bulk conductivity and defect chemistry of acceptor-doped strontium titanate in the quenched state. J Am Ceram Soc. 1991;74(8):1934–40. https://doi.org/10.1111/j.1151-2916.1991.tb07812.x
39. Leng H, Wang YU, Yan Y, Karan SK, Wang K, Li X, et al. Water quenched and acceptor-doped textured piezoelectric ceramics for off-resonance and on-resonance devices. Small. 2023;19:2204454. https://doi.org/10.1002/smll.202204454
40. Jaffe B, Cook WRJ, Jaffe H. Piezoelectric ceramics. Cambridge, MA: Academic Press; 1971.
41. Moon JH, Jang HM. Effect of sintering atmosphere on densification behavior and piezoelectric properties of $Pb(Ni_{1/3}Nb_{2/3})O_3$–$PbTiO_3$–$PbZrO_3$ ceramics. J Am Ceram Soc. 1993;76(2):549–52. https://doi.org/10.1111/j.1151-2916.1993.tb03825.x

42. Oldenkotte M, Kungl H, Eichel R-A, Schönau KA, Kühlein M, Bernard T, et al. Influence of PbO stoichiometry on the properties of PZT ceramics and multilayer actuators. J Am Ceram Soc. 2019;102(9):5401–14. https://doi.org/10.1111/jace.16417
43. Holman RL, Fulrath RM. Intrinsic nonstoichiometry in single-phase $Pb(Zr_{0.5}Ti_{0.5})O_3$. J Am Ceram Soc. (1972);55:192. https://doi.org/10.1111/j.1151-2916.1972.tb11256.x
44. Kingon AI, Clark JB. Sintering of PZT ceramics: I, Atmosphere control. J Am Ceram Soc. 1983;66(4):253–56. https://doi.org/10.1111/j.1151-2916.1983.tb15708.x
45. Kingon AI, Clark JB. Sintering of PZT ceramics: II, Effect of PbO content on densification kinetics. J Am Ceram Soc. 1983;66(4):256–60. https://doi.org/10.1111/j.1151-2916.1983.tb15709.x
46. Xiao Z, Li X, Dong X, Tang J, Wang C, Zhang T, et al. Sintering and electrical properties of commercial PZT powders modified through mechanochemical activation. J Mater Sci. 2018;53:13769–78. https://doi.org/10.1007/s10853-018-2360-y
47. Donnelly NJ, Randall CA. Impedance spectroscopy of PZT ceramics—measuring diffusion coefficients, mixed conduction, and Pb loss. IEEE Trans Ultrason Ferroelectr Freq Control. 2012;59(9):1883–87. https://doi.org/10.1109/TUFFC.2012.2401
48. Prisedsky VV, Shishkovsky VI, Klimov VV. High-temperature electrical conductivity and point defects in lead zirconate-titanate. Ferroelectrics. 1978;17(1):465–68. https://doi.org/10.1080/00150197808236768
49. Tani T, Payne DA. Lead oxide coatings on sol–gel-derived lead lanthanum zirconium titanate thin layers for enhanced crystallization into the perovskite structure. J Am Ceram Soc. 1994;77(5):1242–48. https://doi.org/10.1111/j.1151-2916.1994.tb05398.x
50. Northrop DA. Vaporization of lead zirconate-lead titanate materials. J Am Ceram Soc. 1967;50(9):357–61. https://doi.org/10.1111/j.1151-2916.1968.tb11892.x
51. Pan M-J, Park S-E, Park CW, Markowski KA, Yoshikawa S, Randall CA. Superoxidation and electrochemical reactions during switching in $Pb(Zr,Ti)O_3$ ceramics. J Am Ceram Soc. 1996;79(11):2971–74. https://doi.org/10.1111/j.1151-2916.1996.tb08736.x
52. Akkopru-Akgun B, Wang K, Trolier-Mckinstry S. Links between defect chemistry, conduction, and lifetime in heavily Nb doped lead zirconate titanate films. Appl Phys Lett. 2022;121:162903. https://doi.org/10.1063/5.0117583
53. Härdtl KH, Rau H. PbO vapor pressure in the $Pb(Ti_{1-x}Zr_x)O_3$ system. Solid State Commun. 1969;7(1):41–45. https://doi.org/10.1016/0038-1098(69)90688-7
54. Donnelly NJ, Randall CA. Pb loss in $Pb(Zr,Ti)O_3$ ceramics observed by in situ ionic conductivity measurements. J Appl Phys. 2011;109:104107. https://doi.org/10.1063/1.3585831
55. Donnelly NJ, Randall CA. Mixed conduction and chemical diffusion in a $Pb(Zr_{0.53}, Ti_{0.47})O_3$ buried capacitor structure. Appl Phys Lett. 2010;96:052906. https://doi.org/10.1063/1.3302452
56. Völkl E, Hillebrand P, Fleig J. Resistance variation in donor-doped PZT stacks with Cu inner electrodes under high field stress. J Electroceramics. 2011;27:66–77. https://doi.org/10.1007/s10832-011-9651-x
57. Cui ZH, Gregori G, Ding AL, Guo XX, Maier J. Electrical transport properties of transparent PLZT ceramics: bulk and grain boundaries. Solid State Ionics. 2012;208:4–7. https://doi.org/10.1016/j.ssi.2011.12.001
58. Rödel J, Webber KG, Dittmer R, Jo W, Kimura M, Damjanovic D. Transferring lead-free piezoelectric ceramics into application. J Eur Ceram Soc. 2015;35(6):1659–81. https://doi.org/10.1016/j.jeurceramsoc.2014.12.013
59. Rubinger C, Calado H, Rubinger R, Oliveira H, Donnici C. Lead-free piezoceramics. Nature. 2004;432(4):2023–32. https://doi.org/10.3390/s130202023
60. Xu K, Li J, Lv X, Wu J, Zhang X, Xiao D, et al. Superior piezoelectric properties in potassium—sodium niobate lead-free ceramics. Adv Mater. 2016;28:8519–23. https://doi.org/10.1002/adma.201601859
61. Kato K, Kakimoto K-I, Hatano K, Kobayashi K, Doshida Y. Lead-free Li-modified $(Na,K)NbO_3$ piezoelectric ceramics fabricated by two-step sintering method. J Ceram Soc Jpn. 2014;122(1426):460–63. https://doi.org/10.2109/jcersj2.122.460
62. Li J-F, Wang K, Zhang B-P, Zhang L-M. Ferroelectric and piezoelectric properties of fine-grained $Na_{0.5}K_{0.5}NbO_3$ lead-free piezoelectric ceramics prepared by spark plasma sintering. J Am Ceram Soc. 2006;89(2):706–9. https://doi.org/10.1111/j.1551-2916.2005.00743.x
63. Nakagawa K, Iwasaki M, Fan Z, Roscow JI, Randall CA. The unusual case of plastic deformation and high dislocation densities with the cold sintering of the piezoelectric ceramic $K_{0.5}Na_{0.5}NbO_3$. J Eur Ceram Soc. 2023;43:4015–20. https://doi.org/10.1016/j.jeurceramsoc.2023.02.057
64. Tsuji K, Fan Z, Bang SH, Dursun S, Trolier-Mckinstry S, Randall CA. Cold sintering of the ceramic potassium sodium niobate $(K_{0.5}Na_{0.5})NbO_3$, and influences on piezoelectric properties. J Eur Ceram Soc. 2022;42:105–11. https://doi.org/10.1016/j.jeurceramsoc.2021.10.002
65. Liu Y-X, Qu W, Thong H-C, Zhang Y, Zhang Y, Yao F-Z, et al. Isolated-oxygen-vacancy hardening in lead-free piezoelectrics. Adv Mater. 2022;34:2202558. https://doi.org/10.1002/adma.202202558
66. Malič B, Koruza J, Hreščak J, Bernard J, Wang K, Fisher J, et al. Sintering of lead-free piezoelectric sodium potassium niobate ceramics. Materials. 2015;8(12):8117–46. https://doi.org/10.3390/ma8125449
67. Popovič A, Bencze L, Koruza J, Malič B, Kosec M. Knudsen effusion mass spectrometric approach to the thermodynamics of Na_2O–Nb_2O_5 system. Int J Mass Spectrosc. 2012;309:70–78. https://doi.org/10.1016/j.ijms.2011.08.028
68. Nishiyama H, Martin A, Hatano K, Kishimoto S, Sasaki N, Webber KG, et al. Alkali volatilization of $(Li,Na,K)NbO_3$-based piezoceramics and large-field electrical and mechanical properties. J Ceram Soc Jpn. 2021;129(3):127–34. https://doi.org/10.2109/jcersj2.20201
69. Wang K, Li J-F. $(K, Na)NbO_3$-based lead-free piezoceramics: phase transition, sintering and property enhancement. J Adv Ceram. 2012;1(1):24–37. https://doi.org/10.1007/s40145-012-0003-3
70. Wang Y, Damjanovic D, Klein N, Setter N. High-temperature instability of Li- and Ta-modified $(K,Na)NbO_3$ piezoceramics. J Am Ceram Soc. 2008;91(6):1962–70. https://doi.org/10.1111/j.1551-2916.2008.02392.x
71. Xu Z, Liu Y-X, Azadeh M, Thong H-C, Jiang Y, Yao F-Z, et al. Identifying the interfacial polarization in non-stoichiometric lead-free perovskites by defect engineering. Angew Chem. 2023;62:e202216776. https://doi.org/10.1002/anie.202216776

72. Wang Y, Damjanovic D, Klein N, Hollenstein E, Setter N. Compositional inhomogeneity in Li- and Ta-modified (K,Na)NbO_3 ceramics. J Am Ceram Soc. 2007;90(11):3485–89. https://doi.org/10.1111/j.1551-2916.2007.01962.x
73. Nishiyama H, Ito R, Aizawa T, Goto T, Shimizu H. Mechanical stability of (Li,Na,K)NbO_3-based multilayered piezoceramics with Ag/Pd inner electrodes. J Appl Phys. 2022;132:244102. https://doi.org/10.1063/5.0128389
74. Lévêque G, Marchet P, Levassort F, Tran-Huu-Hue LP, Duclere JR. Lead free (Li,Na,K)(Nb,Ta,Sb)O_3 piezoelectric ceramics: influence of sintering atmosphere and ZrO_2 doping on densification, microstructure and piezoelectric properties. J Eur Ceram Soc. 2011;31:577–88. https://doi.org/10.1016/j.jeurceramsoc.2010.10.031
75. Kawada S, Kimura M, Higuchi Y, Takagi H. (KNa)NbO_3-based multilayer piezoelectric ceramics with nickel inner electrodes. Appl Phys Express. 2009;2(11):7–10. https://doi.org/10.1143/APEX.2.111401
76. Kobayashi K, Doshida Y, Mizuno Y, Randall CA. A route forwards to narrow the performance gap between PZT and lead-free piezoelectric ceramic with low oxygen partial pressure processed ($Na_{0.5}K_{0.5}$)NbO_3. J Am Ceram Soc. 2012;95(9):2928–33. https://doi.org/10.1111/j.1551-2916.2012.05266.x
77. Kobayashi K, Doshida Y, Mizuno Y, Randall CA. Possibility of cofiring a nickel inner electrode in a ($Na_{0.5}K_{0.5}$)NbO_3–LiF piezoelectric actuator. Jpn J Appl Phys. 2013;52(9 Pt 2):5–10. https://doi.org/10.7567/JJAP.52.09KD07
78. Shimizu H, Kobayashi K, Mizuno Y, Randall CA. Advantages of low partial pressure of oxygen processing of alkali niobate: $NaNbO_3$. J Am Ceram Soc. 2014;97(6):1791–96. https://doi.org/10.1111/jace.12815
79. Fisher JG, Rout D, Moon K-S, Kang S-JL. High-temperature X-ray diffraction and Raman spectroscopy study of ($K_{0.5}Na_{0.5}$)NbO_3 ceramics sintered in oxidizing and reducing atmospheres. Mater Chem Phys. 2010;120:263–71. https://doi.org/10.1016/j.matchemphys.2009.11.001
80. Jung Y, Choi S, Kang S. Effect of oxygen partial pressure on grain boundary structure and grain growth behavior in $BaTiO_3$. Acta Mater. 2006;54:2849–55. https://doi.org/10.1016/j.actamat.2006.02.025
81. Shimizu H, Guo H, Reyes-Lillo SE, Mizuno Y, Rabe KM, Randall CA. Lead-free antiferroelectric: $x$$CaZrO_3$–(1 – x)$NaNbO_3$ system ($0 \leqq x \leqq 0.10$). Dalton Trans. 2015;44:10763–72. https://doi.org/10.1039/c4dt03919j
82. Guo H, Shimizu H, Mizuno Y, Randall CA. Strategy for stabilization of the antiferroelectric phase (*Pbma*) over the metastable ferroelectric phase ($P2_1ma$) to establish double loop hysteresis in lead-free $(1-x)$$NaNbO_3$–$x$$SrZrO_3$ solid solution. J Appl Phys. 2015;117:214103. https://doi.org/10.1063/1.4921876
83. Karimi S, Reaney IM, Han Y, Pokorny J, Sterianou I. Crystal chemistry and domain structure of rare-earth doped $BiFeO_3$ ceramics. J Mater Sci. 2009;44:5102–12. https://doi.org/10.1007/s10853-009-3545-1
84. Jaffe H. BNT-BT system for lead-free piezoelectric ceramics. Jpn J Appl Phys. 1991;30(9B):494–98. https://doi.org/10.1111/j.1151-2916.1958.tb12903.x
85. Takenaka T, Nagata H, Hiruma Y. Phase transition temperatures and piezoelectric properties of ($Bi_{1/2}Na_{1/2}$)TiO_3- and ($Bi_{1/2}K_{1/2}$)TiO_3-based bithmuth perovskite lead-free ferroelectric ceramics. IEEE Trans Ultrason Ferroelectr Freq Control. 2009;56(8):1595–612. https://doi.org/10.1109/TUFFC.2009.1224
86. Hejazi MM, Jadidian B, Safari A. Fabrication and evaluation of a single-element $Bi_{0.5}Na_{0.5}TiO_3$-based ultrasonic transducer. IEEE Trans Ultrason Ferroelectr Freq Control. 2012;59(8):1840–47. https://doi.org/10.1109/TUFFC.2012.2389
87. Yang F, Wu P, Sinclair DC. Enhanced bulk conductivity of A-site divalent acceptor-doped non-stoichiometric sodium bismuth titanate. Solid State Ionics. 2017;299:38–45. https://doi.org/10.1016/j.ssi.2016.09.016
88. Li M, Pietrowski MJ, De Souza RA, Zhang H, Reaney IM, Cook SN, et al. A family of oxide ion conductors based on the ferroelectric perovskite $Na_{0.5}Bi_{0.5}TiO_3$. Nat Mater. 2014;13:31–35. https://doi.org/10.1038/NMAT3782
89. Reichmann K, Feteira A, Li M. Bismuth sodium titanate based materials for piezoelectric actuators. Materials (Basel). 2015;8:8467–95. https://doi.org/10.3390/ma8125469
90. Fan Z, Randall CA. Influences of processing temperatures on the nature of polarization phenomena in 85%($Bi_{0.5}Na_{0.5}$)TiO_3–15%$BaTiO_3$ with different strategies of bismuth oxide non-stoichiometry. J Appl Phys. 2023;133:214101. https://doi.org/10.1063/5.0146059
91. Suchanicz J, Kluczewska K, Czaja P, Handke B, Sokolowski M, Węgrzyn A, et al. Influence of sintering conditions on structural, thermal, electric and ferroelectric properties of $Na_{0.5}Bi_{0.5}TiO_3$ ceramics. Phase Transitions. 2018;91(1):26–37. https://doi.org/10.1080/01411594.2017.1341982
92. Seo I-T, Steiner S, Frömling T. The effect of A site non-stoichiometry on 0.94(Na_yBi_x)TiO_3–0.06$BaTiO_3$. J Eur Ceram Soc. 2017;37:1429–36. https://doi.org/10.1016/j.jeurceramsoc.2016.11.045
93. Naderer M, Kainz T, Schütz D, Reichmann K. The influence of Ti-nonstoichiometry in $Bi_{0.5}Na_{0.5}TiO_3$. J Eur Ceram Soc. 2014;34(3):663–67. https://doi.org/10.1016/j.jeurceramsoc.2013.10.010
94. Qiao X-S, Chen X-M, Lian H-L, Zhou J-P, Liu P. Dielectric, ferroelectric, piezoelectric properties and impedance analysis of nonstoichiometric $(Bi_{0.5}Na_{0.5})_{0.94+x}Ba_{0.06}TiO_3$ ceramics. J Eur Ceram Soc. 2016;36:3995–4001. https://doi.org/10.1016/j.jeurceramsoc.2016.06.032
95. Qiao X-S, Chen X-M, Lian H-L, Chen W-T, Zhou J-P, Liu P. Microstructure and electrical properties of nonstoichiometric 0.94($Na_{0.5}Bi_{0.5+x}$)TiO_3–0.06$BaTiO_3$ lead-free ceramics. J Am Ceram Soc. 2016;99:198–205. https://doi.org/10.1111/jace.13941
96. Roy S, Sarah P. Dielectric properties of chemically synthesized PLZT and PZT: diffused phase transition and effect of lead non-stoichiometry. J Phys D Appl Phys. 2007;40:4668–73. https://doi.org/10.1088/0022-3727/40/15/047
97. Acker J, Kungl H, Hoffmann MJ. Influence of alkaline niobium excess on sintering and microstructure of sodium-potassium niobate ($K_{0.5}Na_{0.5}$)NbO_3. 2010;1281:1270–81. https://doi.org/10.1111/j.1551-2916.2010.03578.x
98. Vendrell X, García JE, Rubio-Marcos F, Ochoa DA, Mestres L, Fernández JF. Exploring different sintering atmospheres to reduce nonlinear response of modified KNN piezoceramics. J Eur Ceram Soc. 2013;33(4):825–31. https://doi.org/10.1016/j.jeurceramsoc.2012.09.025
99. Chen C-S, Chen P-Y, Tu C-S, Chang T-L, Chai C-K. The effects of sintering atmosphere on microstructures and electrical

properties of lead-free $(Bi_{0.5}Na_{0.5})TiO_3$-based ceramics. Ceram Int. 2014;40(7):9591–98. https://doi.org/10.1016/j.ceramint.2014.02.034

100. Fan Z, Randall CA. The strange case of enhancing the resistivity by extended sintering time in $(Bi_{0.5}Na_{0.5})TiO_3$–$BaTiO_3$ solid solution. Solid State Commun. 2023;375:115355. https://doi.org/10.1016/j.ssc.2023.115355
101. Muramatsu H, Nagata H, Takenaka T. Quenching effects for piezoelectric properties on lead-free $(Bi_{1/2}Na_{1/2})TiO_3$ ceramics. Jpn J Appl Phys. 2016;55:10TB07. https://doi.org/10.7567/JJAP.55.10TB07
102. Lalitha KV, Wang B, Ren P, Hall DA, Rojac T. Quenching effects and mechanisms in bismuth-based perovskite ferroelectrics. Open Ceram. 2022;10:100259. https://doi.org/10.1016/j.oceram.2022.100259
103. Fan Z, Momjian S, Randall CA. Understanding the depolarization temperature in $(Bi_{0.5}Na_{0.5})TiO_3$-based ferroelectrics. J Eur Ceram Soc. 2023;43:4021–28. https://doi.org/10.1016/j.jeurceramsoc.2023.03.013
104. Fan Z, Randall CA. An overview of oxygen vacancy dynamics in $(1-x)(Bi_{1/2}Na_{1/2})TiO_3$–$xBaTiO_3$ solid solution. J Mater Chem C. 2021;9:10303–8. https://doi.org/10.1039/d1tc02668b
105. Fan Z, Randall CA. Engineering the nature of polarization dynamics in lead-free relaxors based on $(Bi_{1/2}Na_{1/2})TiO_3$. Appl Phys Lett. 2021;119:112906. https://doi.org/10.1063/5.0064160
106. Zeb A, Milne SJ. High temperature dielectric ceramics: a review of temperature-stable high-permittivity perovskites. J Mater Sci Mater Electron. 2015;26:9243–55. https://doi.org/10.1007/s10854-015-3707-7
107. Xu X, Gurav AS, Lessner PM, Randall CA. Robust BME class-I MLCCs for harsh-environment applications. IEEE Trans Ind Electron. 2011;58(7):2636–43. https://doi.org/10.1109/TIE.2010.2089934
108. Devoe A, Trinh H, Dogan F. High temperature dielectric properties of calcium zirconate. Int J Appl Ceram Technol. 2023;20(April):3140–47. https://doi.org/10.1111/ijac.14432
109. Fritsch S, Navrotsky A. Thermodynamic properties of manganese oxides. J Am Ceram Soc. 1996;79(7):1761–68. https://doi.org/10.1111/j.1151-2916.1996.tb07993.x
110. Moos R, Hardtl KH. Defect chemistry of donor-doped and undoped strontium titanate ceramics between 1000°C and 1400°C. J Am Ceram Soc. 1997;80(10):2549–62. https://doi.org/10.1111/j.1151-2916.1997.tb03157.x
111. Fritsch S, Post JE, Suib SL, Navrotsky A. Thermochemistry of framework and layer manganese dioxide related phases. Chem Mater. 1998;10:474–79. https://doi.org/10.1021/cm970104h
112. Tian ZM, Yuan SL, He JH, Wang YQ, Li P, Xie HY, et al. Effects of sintering temperature and atmosphere on magnetism in Mn-doped TiO_2 bulk samples. Solid State Commun. 2007;142:545–49. https://doi.org/10.1016/j.ssc.2007.03.008
113. Kim DJ, Lee MH, Song TK. Comparison of multi-valent manganese oxides (Mn^{4+}, Mn^{3+}, and Mn^{2+}) doping in $BiFeO_3$–$BaTiO_3$ piezoelectric ceramics. J Eur Ceram Soc. 2019;39:4697–704. https://doi.org/10.1016/j.jeurceramsoc.2019.07.013
114. Jeong J, Lee EJ, Han YH. Defect chemistry and electrical degradation of $BaTiO_3$ co-doped with Ho and Mn. J Eur Ceram Soc. 2007;27:1159–63. https://doi.org/10.1016/j.jeurceramsoc.2006.05.025
115. Shay DP, Podraza NJ, Donnelly NJ, Randall CA. High energy density, high temperature capacitors utilizing Mn-doped $0.8CaTiO_3$–$0.2CaHfO_3$ ceramics. J Am Ceram Soc. 2012;95(4):1348–55. https://doi.org/10.1111/j.1551-2916.2011.04962.x

How to cite this article: A. Randall C, Nishiyama H, Shimizu H. Impact of volatility, non-stoichiometry, and atmospheres in perovskite piezoelectric and dielectric materials. J Am Ceram Soc. 2024;107:7921–38. https://doi.org/10.1111/jace.20080